IEEE Access
Multidisciplinary | Rapid Review | Open Access Journal

Received 24 August 2023, accepted 13 September 2023, date of publication 25 September 2023,
date of current version 28 September 2023.

Digital Object Identifier 10.1109/ACCESS.2023.3318548

RESEARCH ARTICLE

An Improved Autonomous Inertial-Based Integrated Navigation Scheme Based on Vehicle Motion Recognition

PEI YU[1], WEI WEI[2], JING LI[2], FANG WANG[2], LILI ZHANG[2], AND ZENGQIANG CHEN[2]

[1]China Fire and Rescue Institute, Beijing 102202, China
[2]College of Information Engineering, Beijing Institute of Petrochemical Technology, Beijing 102617, China

Corresponding author: Wei Wei (weiwei@bipt.edu.cn)

This work was supported in part by the Natural Science Foundation of Ningxia under Grant 2022AAC03757; in part by R&D Program of Beijing Municipal Education Commission under Grant KM202210017006; in part by 2021–2023 Young Talents Promotion Project of Beijing Association for Science and Technology; in part by the Beijing Municipal Natural Science Foundation under Grant 4214070; in part by the University-Industry Collaborative Education Program under Grant 220607039172210, Grant 220607039282934, and Grant 22107153134955; and in part by the Research Project of Digital Education in Beijing under Grant BDEC2022619048.

ABSTRACT The autonomous navigation technology of INS has always attracted the attention of many scholars. In satellite-denied environment, making full use of the auxiliary sensors with autonomous characteristics can suppress the dynamic error generated by INS in autonomous navigation effectively. However, auxiliary sensors like an odometer (OD) and laser doppler velocimeter (LDV) will cause instability to the navigation system. To solve the above problems, we propose an improved autonomous inerital-based integrated navigation scheme utilizing vehicle motion recognition. The main research work can be summarized as: (1) Non-holonomic constrained velocity model and tri-axis zero velocity model has been established for inertial-based integrated navigation model. (2) Vehicle motion state recognition method has been proposed utilizing the IMU data. As shown in the experimental results, the proposed method can estimate the IMU biases and increase the positioning accuracy effectively as compared with the traditional methods.

INDEX TERMS In-motion alignment, strapdown inertial navigation system (SINS), odometer (OD), backtracking.

I. INTRODUCTION

The autonomous navigation technology of strapdown inertial navigation system (INS) has always attracted the attention of many scholars [1], [2], [3]. In satellite-denied environment, making full use of the auxiliary sensors with autonomous characteristics can effectively suppress the dynamic error generated by the INS in autonomous navigation. In addition to the aforementioned odometer, auxiliary sensors that can provide autonomous information in the land field also includes electronic maps and barometric altimeters (BA). The electronic map can provide accurate track information, and the barometric altimeter can stably provide high-precision elevation information, thus making it possible for INS to provide higher-precision positioning and navigation. In addition, when the use of various auxiliary sensors is limited, velocity constraints are an important auxiliary means of INS, including Tri-axis Zero Velocity (TZV) and vehicle kinematics constraints (also known as non-holonomic constraints, Non-Holonomic Constraints, NHC) [4], [5]. Therefore, based on various auxiliary observation information, it is of great significance to study the autonomous navigation method of INS in the satellite-denied environment to realize multi-mode and multi-task autonomous navigation and improve the positioning accuracy of long-distance land navigation [6], [7].

In the application field of autonomous navigation that does not depend on satellite navigation, the navigation error of INS accumulates with time, so INS needs to introduce external auxiliary information to realize autonomous navigation.

The associate editor coordinating the review of this manuscript and approving it for publication was Kegen Yu.

As a typical INS autonomous navigation method, zero-velocity correction has been widely used in engineering. The commonly used methods include the curve fitting method [8] and Kalman filtering method [9]. Since zero velocity correction is based on the curve fitting method, the scheme ignores the coupling between inertial navigation error propagation channels and cannot reflect the change in the internal state of the system. The Kalman filter method is based on the optimal state estimation of the inertial navigation system error model, so it has been widely used. Among foreign land inertial navigation products, Draper's APTS series adopts a 20-dimensional state real-time Kalman filter, Honeywell's GEO-SPIN series adopts a 27-dimensional state real-time Kalman filter and adds a smoothing filter algorithm; Ferranti's FILS series adopts 10-dimensional state The LASS series of Litton Company adopts the real-time Kalman filter of "14+4" dimensional state to correct the horizontal error and vertical error respectively [10]; in 2001, Dissanayake proposed the vehicle kinematics constraint concept, and use it as auxiliary information for low-precision SINS when GPS is out of lock [11]; The introduction of onboard Dynamic Zero Velocity Update (DZUPT) provides a new idea for the zero-velocity correction of SINS, but does not mention how to carry out effective vehicle motion state detection [12].

In addition to zero velocity correction, INS has many other autonomous navigation methods. Among them, the odometer and barometric altimeter with independent characteristics is typical external auxiliary sensors of INS. Due to the sensitive technical information involved, many countries (like USA, German, France, etc) only disclose the technical indicators of INS/OD autonomous navigation and do not disclose technical details. Many domestic scholars have done a lot of research in this field. In 2006, Yan *et al*. systematically summarized the numerical update algorithm of SINS and dead reckoning system, and derived the SINS/OD integrated navigation error model. To improve the system's fault tolerance and reduce the amount of calculation, Fu *et al*. proposed the SINS/OD incremental integrated navigation method, and established the odometer incremental error model [13], [14], and introduced the BA to provide elevation information. Due to the constraints of inertial sensors' accuracy, mileage measurement accuracy, and driving road conditions, there is limited room for improvement in the horizontal positioning accuracy of the INS/OD autonomous navigation system. In recent years, with the development of computer technology and the popularization of map navigation, the geographic information system based on electronic maps has been gradually improved. Since the digital information of electronic maps can be stored in hardware in advance, INS/map matching (Map Matching, MM) can also be used as an autonomous navigation method. Currently, map matching algorithms include point-to-point matching algorithm [15], point-to-line matching algorithm [16], line-to-line matching algorithm [17], filtering algorithm [18], probabilistic Algorithm [19], fuzzy logic algorithm [20], etc. Many scholars have utilized NHC method in complex integrated navigation systems. Won et al. utilized magnetometer with NHC method for vehicular navigation system [21]. Wang et al. utilized NHC method in INS/GNSS tightly coupled integrated navigation system to improve the navigation accuracy [22]. In [23], the authors analyzed the prerequisite of NHC method and use the NHC method in satellite-denied areas. Zhao and Quan used regularized softmax regression in GNSS/INS integrated navigation system with NHC method [24]. However, the above methods cannot eliminate the radial error and vertical error of INS along the road at the same time, and a more effective method needs to be further studied.

However, the auxiliary sensors will cause instability in the navigation system. The skidding and sideslipping of the vehicle will have a greater side effect in the process of odometer integrated navigation. The failure of the odometer will also have a great impact on the navigation accuracy. As for map-matching, first, map matching has a certain accuracy rate, which cannot guarantee correct matching every time; second, map matching relies on big data information, and needs to be updated in real time, and the cost is high; third, in some occasions, such as non-road operation, in this case, map matching cannot be used. When the odometer, barometric altimeter, electronic map, and other external auxiliary equipment equipped with the vehicle fail or the vehicle is not equipped with external auxiliary equipment, the velocity constraint information can be used to suppress the divergence of INS navigation accuracy. Typical velocity constraints include TZV information and NHC information. When the vehicle is stationary, the TZV information is valid. At this time, the traditional zero-velocity correction method can be used to correct the error of the INS, but the shortcomings of the zero-velocity correction are also obvious: the calibration residual error of the INS is stimulated by the dynamic environment of the vehicle. It will lead to the weakening of the velocity error propagation law, the zero velocity correction of long time intervals will lead to the nonlinearity of the model, and the zero velocity correction of short time intervals will reduce the maneuverability of the vehicle. When the vehicle is stationary or does not jump or skid while the vehicle is running, the NHC information will continue to be valid. The shortest measurement information update sampling time can be set to the INS data update sampling time. The measurement update frequency is significantly increased, but when the vehicle is long driving along a straight line will result in the accumulation of longitudinal positioning errors in the body coordinate system.

To solve the above problems, we propose an improved autonomous inertial-based integrated navigation scheme utilizing vehicle motion recognition. The main research work can be summarized as: (1) Non-holonomic constrained velocity model and tri-axis zero velocity model has been established for inertial-based integrated navigation model. (2) Vehicle motion state recognition method has been proposed utilizing the IMU data. The novelty of this study

lies in that we propose a stable judgment for the vehicle motion state. A reliable motion state judgement can help the autonomous integrated navigation system switch to a reasonable working mode in time, so that improve the navigation accuracy. Experimental results show that the proposed method can effectively estimate the IMU biases, and increase the positioning accuracy compared with the traditional INS/NHC integrated navigation method.

The remainder of this paper is organized as follows: Section II gives Non-holonomic constrained velocity model. In section III, we propose the INS/TZV/NHC filtering algorithm design based on vehicle motion recognition. Vehicle experimental analysis is carried out in Section IV to verify the effectiveness of the proposed method. In Section V, we give the conclusions.

II. NON-HOLONOMIC CONSTRAINED VELOCITY MODEL

A. REFERENCE DEFINITIONS

In this paper, the reference frames in the proposed INS/NHC/TZV algorithm which utilized are defined as the following:

n frame: The East-North-Up geodetic orthogonal reference frame, which is coincides with east-north-upward (E-N-U) frame.

b frame: The inertial measurement unit (IMU) orthogonal frame aligned with IMU's Right-Forth-Up axes, and we described it as body frame in this paper, the x-axis is coincides with the sensitive axis of x-gyroscope.

m frame: The experimental car Right-Forth-Up orthogonal frame, which is also known as vehicle frame in this paper.

To complete the establishment of the state space model of the strapdown INS/TZV/NHC autonomous navigation system, it is first necessary to establish a velocity measurement model with non-holonomic constraints. When the INS is installed on the vehicle, if the vehicle does not slip or jump during driving, the condition of the non-holonomic constraint is satisfied, that is, the velocity measurement point O_H of the non-holonomic constraint is in the axis ox_m and axis oz_m direction of the vehicle body coordinate system. $\boldsymbol{v}_H^m$ denotes the velocity of the vehicle projected in *m*-frame. The sum of the velocity projection components v_{Hx}^m and v_{Hy}^m are 0, as shown in FIG.1. Therefore, virtual velocity observations in both directions can still be obtained while the vehicle is moving.

Considering the influence of the installation deviation angles $\tilde{\alpha}_\theta, \tilde{\alpha}_\psi$ and the installation lever arm $\tilde{\boldsymbol{L}}_H^b$, the projection component $\tilde{\boldsymbol{v}}_{HI}^m$ of the INS solution velocity $\tilde{\boldsymbol{v}}_I^n$ at the point O_H in the vehicle body coordinate system (*m*-frame) is shown in the following equation:

$$\tilde{\boldsymbol{v}}_{HI}^m = \tilde{\boldsymbol{C}}_b^m \tilde{\boldsymbol{C}}_n^b \tilde{\boldsymbol{v}}_I^n + \boldsymbol{\omega}_{eb}^b \times \tilde{\boldsymbol{L}}_H^b \tag{1}$$

where $\tilde{\boldsymbol{C}}_n^b = \boldsymbol{C}_n^b [I + (\phi^n \times)]$, $\tilde{\boldsymbol{C}}_b^m = \boldsymbol{C}_b^m [I + (\delta\boldsymbol{\alpha} \times)]$ is the installation matrix between INS and the vehicle. $\delta\boldsymbol{\alpha} = \begin{bmatrix} \delta\alpha_\theta & 0 & \delta\alpha_\psi \end{bmatrix}^T$, $\tilde{\boldsymbol{L}}_H^b = \boldsymbol{L}_H^b + \delta\boldsymbol{L}_H^b$. $\tilde{\boldsymbol{C}}_n^b$ denotes the calculated attitude transform matrix from *b*-frame to *n*-frame with calculation errors (misalignment errors). $\boldsymbol{\omega}_{eb}^b$ denotes the angular velocity of the IMU in the *e*-frame. *b*-frame denotes the body frame of the IMU, and *n*-frame is the navigation frame which coincides with East-North-Upward (E-N-U). *e*-frame denotes Earth-Centered Earth Fixed (ECEF) orthogonal reference frame.

Considering the above errors, we can obtain:

$$\begin{aligned}
\tilde{\boldsymbol{v}}_{HI}^m &= \boldsymbol{C}_b^m [I + (\delta\boldsymbol{\alpha} \times)] \boldsymbol{C}_n^b \left[I + \left(\phi^n \times\right)\right] \left(\boldsymbol{v}_I^n + \delta\boldsymbol{v}_I^n\right) \\
&\quad + \boldsymbol{\omega}_{eb}^b \times \left(\boldsymbol{L}_H^b + \delta\boldsymbol{L}_H^b\right) \\
&\approx \left(\boldsymbol{C}_b^m \boldsymbol{C}_n^b \boldsymbol{v}_I^n + \boldsymbol{\omega}_{eb}^b \times \boldsymbol{L}_H^b\right) + \boldsymbol{C}_b^m \boldsymbol{C}_n^b \delta\boldsymbol{v}_I^n \\
&\quad + \boldsymbol{C}_b^m \boldsymbol{C}_n^b \left(\phi^n \times\right) \boldsymbol{v}_I^n + \boldsymbol{C}_b^m (\delta\boldsymbol{\alpha} \times) \boldsymbol{C}_n^b \boldsymbol{v}_I^n + \boldsymbol{\omega}_{eb}^b \times \delta\boldsymbol{L}_H^b \\
&= \boldsymbol{v}_{HI}^m + \boldsymbol{C}_b^m \boldsymbol{C}_n^b \delta\boldsymbol{v}_I^n - \boldsymbol{C}_b^m \boldsymbol{C}_n^b \left(\boldsymbol{v}_I^n \times\right) \phi^n \\
&\quad - \boldsymbol{C}_b^m \left(\boldsymbol{C}_n^b \boldsymbol{v}_I^n\right) \times \delta\boldsymbol{\alpha} + \boldsymbol{\omega}_{eb}^b \times \delta\boldsymbol{L}_H^b \\
&= \boldsymbol{v}_{HI}^m + \boldsymbol{M}_{H1}\phi^n + \boldsymbol{M}_{H2}\delta\boldsymbol{v}_I^n + \boldsymbol{M}_{H3}\delta\boldsymbol{\alpha} + \boldsymbol{M}_{H4}\delta\boldsymbol{L}_H^b
\end{aligned} \tag{2}$$

where $\boldsymbol{M}_{H1} = -\boldsymbol{C}_b^m \boldsymbol{C}_n^b \left(\boldsymbol{v}_I^n \times\right)$ $\boldsymbol{M}_{H2} = \boldsymbol{C}_b^m \boldsymbol{C}_n^b$ $\boldsymbol{M}_{H3} = -\boldsymbol{C}_b^m \left(\boldsymbol{C}_n^b \boldsymbol{v}_I^n\right) \times$ $\boldsymbol{M}_{H4} = \boldsymbol{\omega}_{eb}^b \times$, and $\delta\tilde{\boldsymbol{v}}_{HI}^m$ can be described as:

$$\delta\boldsymbol{v}_{HI}^m = \boldsymbol{M}_{H1}\phi^n + \boldsymbol{M}_{H2}\delta\boldsymbol{v}_I^n + \boldsymbol{M}_{H3}\delta\boldsymbol{\alpha} + \boldsymbol{M}_{H4}\delta\boldsymbol{L}_H^b \tag{3}$$

So far, the velocity measurement model with non-holonomic constraints has been established.

III. INS/TZV/NHC FILTERING ALGORITHM DESIGN BASED ON VEHICLE MOTION RECOGNITION

A. INS/TZV/NHC AUTONOMOUS NAVIGATION STATE SPACE MODEL

When carrying out INS/TZV/NHC error modeling, on the basis of the traditional 15-dimensional zero-velocity corrected Kalman filter [26], consider the azimuth installation deflection angle $\delta\alpha_\psi$ and pitch installation deflection angle $\delta\alpha_\theta$ between the INS and the vehicle body [27], and the strapdown The installation lever arm error $\delta\boldsymbol{L}_H$ between INS and the equivalent kinematic constraint measurement point O_H [28], the state space model can be expanded to 20 dimensions, and the state vector $\boldsymbol{X}_{TH}$ is as follows:

$$\begin{aligned}
\boldsymbol{X}_{TH} = \Big[&(\boldsymbol{\phi}^n)^T \ \left(\delta\boldsymbol{v}_I^n\right)^T \ (\delta\boldsymbol{p})^T \\
&\left(\boldsymbol{\varepsilon}^b\right)^T \ \left(\nabla^b\right)^T \ \delta\alpha_\theta \ \delta\alpha_\psi \ \delta\boldsymbol{L}_H^b \Big]^T
\end{aligned} \tag{4}$$

In the INS/TZV/NHC autonomous navigation state equation, $\boldsymbol{F}_{TH}$ is defined as the state transition matrix, $\boldsymbol{G}_{TH}$ is the system noise driving matrix, and $\boldsymbol{W}_{TH} = \begin{bmatrix} \boldsymbol{\varepsilon}_w^b & \nabla_w^b \end{bmatrix}^T$ is the system excitation noise matrix. The INS/TZV/NHC autonomous navigation state equation can be expressed as:

$$\dot{\boldsymbol{X}}_{TH} = \boldsymbol{F}_{TH}\boldsymbol{X}_{TH} + \boldsymbol{G}_{TH}\boldsymbol{W}_{TH} \tag{5}$$

where $\boldsymbol{F}_{TH} = \begin{bmatrix} \boldsymbol{F}_{15\times15} & 0_{15\times5} \\ 0_{5\times15} & 0_{5\times5} \end{bmatrix}$, $\boldsymbol{G}_{TH} = \begin{bmatrix} -\boldsymbol{C}_b^n & 0_{3\times3} \\ 0_{3\times3} & \boldsymbol{C}_b^n \\ & 0_{14\times6} \end{bmatrix}$. The detailed elements of $\boldsymbol{F}_{TH}$ are shown in [25].

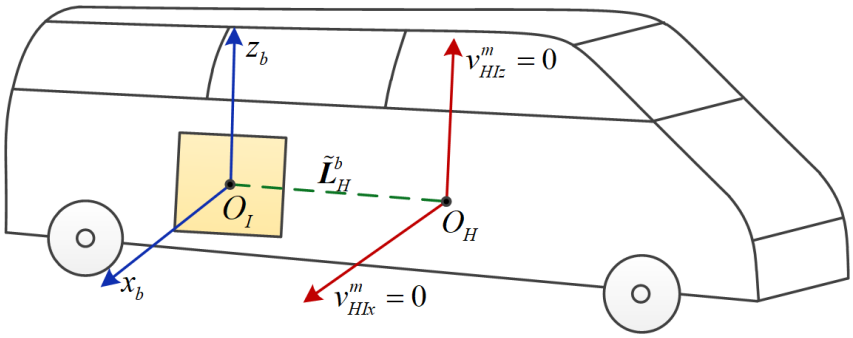

FIGURE 1. Schematic diagram of the relationship between INS and vehicle kinematics constraint installation.

When constructing INS/TZV/NHC autonomous navigation measurement equations, TZV information and NHC information should be considered as the timing of measurement: when the vehicle is stationary, TZV information is valid; when the vehicle is stationary or moving without sideslip and jumping, the NHC information is valid, but compared with the NHC information, the TZV information constraints are more complete, so the TZV is used as the measurement when the vehicle is stationary; The noise of NHC information is relatively large, and the reliability is not high, so it is not suitable for measurement and update. The following introduces the measurement equations in the stationary state and the moving state of the vehicle respectively, laying the foundation for the subsequent INS/TZV/NHC filter algorithm design based on the detection of the moving state of the vehicle.

(1) INS/TZV Autonomous Navigation Measurement Equation in Static Vehicle State: The TZV information is valid when the vehicle is stationary, and the difference between the strapdown INS real-time calculated velocity $\left[\tilde{v}^n_{IE}\ \tilde{v}^n_{IN}\ \tilde{v}^n_{IU}\right]^T$ and the TZV information is used as a measurement to obtain:

$$\boldsymbol{Z}_T=\begin{bmatrix}\tilde{v}^n_{IE}\\ \tilde{v}^n_{IN}\\ \tilde{v}^n_{IU}\end{bmatrix}-\begin{bmatrix}0\\0\\0\end{bmatrix}=\begin{bmatrix}\tilde{v}^n_{IE}\\ \tilde{v}^n_{IN}\\ \tilde{v}^n_{IU}\end{bmatrix}=\begin{bmatrix}\delta v^n_{IE}\\ \delta v^n_{IN}\\ \delta v^n_{IU}\end{bmatrix} \tag{6}$$

INS/TZV autonomous navigation measurement equation is recorded as:

$$\boldsymbol{Z}_T=\boldsymbol{H}_T\boldsymbol{X}_{TH}+\boldsymbol{V}_T \tag{7}$$

where V_T represents the measurement noise of the TZV, R_T is the noise variance matrix of the measurement noise V_T; H_T represents the measurement matrix, which can be expressed according to Eq. (6) as:

$$\boldsymbol{H}_T=\left[0_{3\times3}\ \boldsymbol{I}_{3\times3}\ 0_{3\times14}\right] \tag{8}$$

At this time, the dynamic error correction mode of INS is zero velocity correction mode.

(2) INS/NHC autonomous navigation measurement equation in vehicle motion state:

The NHC information is valid when the vehicle has no sideslip, jump and fast azimuth maneuver. Taking the difference between the projection of the velocity $\left[\tilde{v}^m_{HIx}\ \tilde{v}^m_{HIz}\right]^T$ of the x axis and the z axis of the axis at the point O_H calculated in real-time by the INS under the system and the vehicle lateral and vertical zero-velocity constraint information as the measurement, it is obtained as:

$$\begin{aligned}\boldsymbol{Z}_H&=\begin{bmatrix}\delta v^m_{HIx}\\ \delta v^m_{HIx}\end{bmatrix}=\begin{bmatrix}\tilde{v}^m_{HIx}\\ \tilde{v}^m_{HIx}\end{bmatrix}-\begin{bmatrix}0\\0\end{bmatrix}=\begin{bmatrix}\tilde{v}^m_{HIx}\\ \tilde{v}^m_{HIx}\end{bmatrix}\\&=\tilde{\boldsymbol{C}}^m_b\tilde{\boldsymbol{C}}^b_n\begin{bmatrix}\tilde{v}^n_{IE}\\ \tilde{v}^n_{IU}\end{bmatrix}+\begin{bmatrix}-\omega^b_{ebz}\tilde{L}^b_{Hy}+\omega^b_{eby}\tilde{L}^b_{Hz}\\ -\omega^b_{eby}\tilde{L}^b_{Hx}+\omega^b_{ebx}\tilde{L}^b_{Hy}\end{bmatrix}\end{aligned} \tag{9}$$

INS/NHC autonomous navigation measurement equation is recorded as:

$$\boldsymbol{Z}_H=\boldsymbol{H}_H\boldsymbol{X}_{TH}+\boldsymbol{V}_H \tag{10}$$

where $\boldsymbol{V}_H$ represents the measurement noise of NHC, $\boldsymbol{R}_H=E\left[\boldsymbol{V}_H\boldsymbol{V}_H^T\right]$ represents the noise variance matrix $\boldsymbol{V}_H$ of the measurement noise;H_H represents the measurement matrix, which can be expressed according to Eq. (9) and Eq. (10):

$$\begin{aligned}\boldsymbol{H}_H=\Bigg[&\begin{matrix}\boldsymbol{M}_{H1}(1,:)\ \boldsymbol{M}_{H2}(1,:)\\ \boldsymbol{M}_{H1}(1,:)\ \boldsymbol{M}_{H2}(3,:)\end{matrix}\ 0_{2\times9}\\&\begin{matrix}\boldsymbol{M}_{H3}(1,1)\ \boldsymbol{M}_{H3}(1,3)\ \boldsymbol{M}_{H4}(1,:)\\ \boldsymbol{M}_{H3}(3,1)\ \boldsymbol{M}_{H3}(3,3)\ \boldsymbol{M}_{H4}(3,:)\end{matrix}\Bigg]\end{aligned} \tag{11}$$

At this time, the dynamic error correction mode of the INS is the dynamic zero velocity correction mode.

B. VEHICLE MOTION STATE RECOGNITION

Vehicle motion state detection is particularly critical to the selection of measurement equations. The vehicle motion state detection criteria include the zero-velocity criterion and the valid NHC information criterion, which will be introduced respectively below.

(1) Zero velocity criterion 1–Heading Constraint Criterion (HCC):

When the vehicle is stationary, the horizontal attitude of the INS is easily affected by the external environment and people getting on and off the vehicle, so it should not be used as a zero-velocity criterion; the heading maintenance accuracy

of the medium and high-precision INS is very high, and the extreme value of the heading change in the sliding window $[t_{j-1}, t_j]$ can be introduced And a reasonable threshold is used as the zero velocity criterion, that is, the heading constraint criterion. Considering the impact of vehicle idling velocity and the control accuracy of the shafting mechanism of the indexing mechanism, the heading constraint threshold should not exceed 0.1mil in the application of medium and high-precision INS. The course constraint criterion includes two sub-criteria, as shown in Eq. (12):

$$\begin{cases} C11 : \tilde{\psi}_{max} - \tilde{\psi}_{min} < \Delta\psi_{Th} \\ C12 : \tilde{\psi}_{max} - \tilde{\psi}_{min} > 360^\circ - \Delta\psi_{Th} \end{cases} \tag{12}$$

In the formula, $\tilde{\psi}_{max}$ and $\tilde{\psi}_{min}$ represent the maximum and minimum heading angles in the sliding window $[t_{j-1}, t_j]$ respectively, and $t_j - t_{j-1}$ is usually taken as the measurement period of the INS/TZV autonomous navigation system, and $T_M = t_j - t_{j-1} = 1s$ is used in this section; $\Delta\psi_{Th}$ is the heading change threshold set in the sliding window $[t_{j-1}, t_j]$. It should be pointed out that the situation $C12$ is the critical state of the heading angle definition domain. Before each measurement update, if $C11$ and $C12$ one of the conditions is satisfied, the INS can be considered to meet the course constraint criterion, and the course constraint criterion is abbreviated as $C11 \parallel C12$.

(2) Zero velocity criterion 2–Inertial Information Constraint Criterion (IMCC)

When the vehicle is stationary, the gyroscope and the accelerometer are mainly sensitive to the earth's rotation angular velocity information and the support force, in which the support force is equal to the gravity mode and opposite in direction; in addition, the gyro and the accelerometer are respectively sensitive to the vibration angular velocity when the vehicle is idling, and acceleration information. Note that the modulus of the angular velocity information of the gyroscope $\left|\tilde{\omega}_{ib}^b(t_i)\right|$ and the specific force information of the accelerometer $\left|\tilde{\boldsymbol{f}}_{sf}^b(t_i)\right|$ at time within $t_i\,(i = 1, 2, \cdots, N)$ the sliding window $[t_{j-1}, t_j]$ are:

$$\begin{cases} \left|\boldsymbol{\omega}_{ib}^b(t_i)\right| = \sqrt{\left[\tilde{\omega}_{ibx}^b(t_i)\right]^2 + \left[\tilde{\omega}_{iby}^b(t_i)\right]^2 + \left[\tilde{\omega}_{ibz}^b(t_i)\right]^2} \\ \left|\tilde{\boldsymbol{f}}_{sf}^b(t_i)\right| = \sqrt{\left[\tilde{f}_{sfx}^b(t_i)\right]^2 + \left[\tilde{f}_{sfy}^b(t_i)\right]^2 + \left[\tilde{f}_{sfz}^b(t_i)\right]^2} \end{cases} \tag{13}$$

where $\tilde{\boldsymbol{\omega}}_{ib}^b$ denotes the angular velocity in the i-frame measured by the three gyroscopes. $\tilde{\boldsymbol{f}}_{ib}^b$ is the specific force in the i-frame by the three accelerometers.

The sampling information of the gyroscope and the accelerometer at a certain moment in the actual project is the angular increment information and the velocity incremental information, which can be divided by the sampling time to obtain the angular velocity information (rad/s) and specific force information (m/s^2).

The maximum and average values of the gyro and accelerometer output in the sliding window $[t_{j-1}, t_j]$ and a reasonable threshold are used as the zero velocity criterion, that is, the inertial information constraint criterion. Information is calculated, and on this basis, it can be adjusted according to the actual vehicle dynamic environment. The inertial information constraint criterion includes four sub-criteria, as shown as follows:

$$\begin{cases} C21 : \left|\tilde{\omega}_{ib}^b\right|_{max} = \underset{i=1}{\overset{N}{max}} \left|\tilde{\omega}_{ib}^b(t_i)\right| < \omega_{Th,max} \\ C22 : \left|\tilde{\omega}_{ib}^b\right|_{mean} = \dfrac{1}{N}\sum_{i=1}^{N} \left|\tilde{\omega}_{ib}^b(t_i)\right| < \omega_{Th,mean} \\ C23 : \left|\tilde{\boldsymbol{f}}_{sf}^b\right|_{max} = \underset{i=1}{\overset{N}{max}} \left|\tilde{\boldsymbol{f}}_{sf}^b(t_i)\right| < f_{Th,max} \\ C24 : \left|\tilde{\boldsymbol{f}}_{sf}^b\right|_{mean} = \dfrac{1}{N}\sum_{i=1}^{N} \left|\tilde{\boldsymbol{f}}_{sf}^b(t_i)\right| < f_{Th,mean} \end{cases} \tag{14}$$

where $\left|\tilde{\omega}_{ib}^b\right|_{max}$ and $\left|\tilde{\omega}_{ib}^b\right|_{mean}$ represent the maximum modulus and average modulus output by the gyroscope in the sliding window $[t_{j-1}, t_j]$ respectively; $\omega_{Th,max}$ and $\omega_{Th,mean}$ represent the maximum angular velocity modulus threshold and the average angular velocity modulus threshold set in the sliding window; $\left|\tilde{\boldsymbol{f}}_{sf}^b\right|_{max}$ and $\left|\tilde{\boldsymbol{f}}_{sf}^b\right|_{mean}$ represent the maximum output of the accelerometer in the sliding window The modulus value and the average modulus value; $f_{Th,max}$ and $f_{Th,mean}$ represent the maximum acceleration modulus threshold and the average acceleration modulus threshold set in the sliding window, respectively. Before each measurement update, if $C21$, $C22$, $C23$ and $C24$ are simultaneously established, it can be considered that the INS meets the inertial information constraint criterion, and the inertial information constraint criterion is abbreviated as $C21\&C22\&C23\&C24$.

(3) NHC information criterion (NHC Criterion, NHCC)

In the field of land use, the horizontal attitude of the vehicle is small. When the vehicle jumps under the condition of large maneuvering, the measured specific force of the INS's z axial accelerometer $\tilde{f}_{sfz}^b$ will change greatly, which $\tilde{f}_{sfz}^b$ can be judged by setting the high and low thresholds; The sliding phenomenon is easy to occur when the vehicle is maneuvering rapidly in azimuth. At this time, the absolute value of the angular velocity $\left|\tilde{\omega}_{ibz}^b\right|$ measured by the z axis gyro is relatively large, and it can be judged by setting the maximum angular velocity threshold $\left|\tilde{\omega}_{ibz}^b\right|$. According to the above two situations, the effective criterion of vehicle NHC information is shown in Eq. (15):

$$\begin{cases} C31 : f_{Thz,min}^b < \dfrac{1}{N}\sum_{i=1}^{N} \tilde{f}_{sfz}^b(t_i) < f_{Thz,max}^b \\ C32 : \dfrac{1}{N}\sum_{i=1}^{N} \left|\tilde{\omega}_{ibz}^b(t_i)\right| < \omega_{Thz,max}^b \end{cases} \tag{15}$$

where $\tilde{f}_{sfz}^b(t_i)$ represents the measured specific force of the z axial accelerometer at the sampling time t_i (usually a positive value in actual situations); $f_{Thz,min}^b$ and $f_{Thz,max}^b$ represent the minimum and maximum thresholds of the specific force

measured by the z axial accelerometer at each sampling time; $\left|\tilde{\omega}_{ibz}^{b}(t_i)\right|$ represents the absolute value of angular velocity measured by the z axial gyroscope at the sampling time t_i; $\omega_{Thz,max}^{b}$ represents the maximum threshold set by the z axial gyro measurement angular velocity at each sampling time. Before each measurement update, if $C31$ and $C32$ are established at the same time, it can be considered that the INS meets the NHCC test, and the condition for the establishment of the NHCC test is abbreviated as $C31\&C32$.

Combined with the above analysis, the flow chart of INS/TZV/NHC filter algorithm design based on vehicle motion state detection is shown in FIG.2. The vehicle motion state detection part mainly includes HCC detection module, IMCC detection module, and NHCC detection module. The filtering part mainly includes INS/TZV measurement update, INS/NHC measurement update, and INS/TZV/NHC time update.

When the HCC test and IMCC test pass at the same time, the vehicle is considered to be in a static state. At this time, the measurement update can be performed at the INS/TZV measurement update time point; otherwise, the vehicle is moving. When the NHCC test passes, the NHC information is displayed to be valid, the measurement update can be performed at the INS/NHC measurement update time point at this time; when the NHCC test fails, the NHC information is considered invalid, and only the INS/TZV/NHC time update is performed at this time.

Because the factors affecting navigation accuracy are mainly IMU biases and attitude accuracy. We mainly analyze the observability of the $\boldsymbol{\phi}^n$, $\boldsymbol{\nabla}^b$ and $\boldsymbol{\varepsilon}^b$. First, we have:

$$\dot{\boldsymbol{Z}}_H \approx \begin{bmatrix} \delta\dot{v}_{HIx}^{b} \\ \delta\dot{v}_{HIz}^{b} \end{bmatrix} = \begin{bmatrix} -g\phi_y^b + \nabla_x^b \\ \nabla_z^b \end{bmatrix} \tag{16}$$

When the vehicle does not have acceleration, it can be seen directly and observable according to Eq. (16). When the vehicle has azimuth maneuvering, the change of the attitude matrix can be known and observed. so that ∇_x^b and ∇_y^b can be separated. Through coordinate system conversion, ϕ_x^b can be Observed, and the degree of observability is improved.

Similarly, we have:

$$\begin{aligned} \dot{\phi}^n &= \phi^n \times \boldsymbol{\omega}_{in}^n + \delta\boldsymbol{\omega}_{in}^n - \boldsymbol{C}_b^n\boldsymbol{\varepsilon}^b \approx -\boldsymbol{\omega}_{ie}^n \times \phi^n - C_b^n\boldsymbol{\varepsilon}^b \\ &= \begin{bmatrix} 0 & \omega_{ie}sinL & -\omega_{ie}cosL \\ -\omega_{ie}sinL & 0 & 0 \\ \omega_{ie}cosL & 0 & 0 \end{bmatrix} \begin{bmatrix} \phi_E^n \\ \phi_N^n \\ \phi_U^n \end{bmatrix} - C_b^n \begin{bmatrix} \varepsilon_x^b \\ \varepsilon_y^b \\ \varepsilon_z^b \end{bmatrix} \\ &= \begin{bmatrix} \phi_N^n\omega_{ie}sinL - \phi_U^n\omega_{ie}cosL \\ -\phi_E^n\omega_{ie}sinL \\ \phi_E^n\omega_{ie}cosL \end{bmatrix} - \begin{bmatrix} \varepsilon_E^n \\ \varepsilon_N^n \\ \varepsilon_U^n \end{bmatrix} \end{aligned} \tag{17}$$

Based on the theory of inertial navigation, since ε_x^b and ε_y^b cause the changes of ϕ_E^b and ϕ_N^b, and the changes of ϕ_E^b and ϕ_N^b can only be reflected in the speed measurement after the transformation of the attitude matrix, therefore, on the basis of ϕ_N^b and ϕ_E^b being observable, ε_x^b and ε_y^b still need a certain time can be estimated, and the observability of ε_z^b is the worst.

IV. VEHICLE EXPERIMENT ANALYSIS

A. EXPERIMENTAL SETUP

This experiment is aimed at prototype verification of INS/OD autonomous navigation and INS/TZV/NHC autonomous navigation. The accuracy of the gyroscopes is $0.01°/h$, and the accuracy of accelerometers is $50\mu g$. The GPS we utilize in this experiment is with an accuracy of 1m (1σ). The vehicle-mounted platform for small passenger vehicles is shown in FIG.3. The length, width, and height of the vehicle body are about 5.3m×2.3m×2.0m; the INS attitude, velocity, and vehicle trajectory are shown in FIG.4 (a) and FIG.4 (b) respectively. As shown in FIG.4 (c), the vehicle is driving on the Sixth Ring Road in Beijing, which is approximately a closed-loop path (denoted as path 1). The total driving distance is about 187km, the height difference is about 82m, and the driving time is about 4.1h.

The starting point and ending point of path 2 are Qufu City and Zhengding County respectively. The driving trajectory is an open-loop path. The total driving distance is about 450km, the height difference is about 200m, and the duration is about 7.57h.

B. EXPERIMENT ANALYSIS OF PATH 1

At the start of INS/TZV/NHC autonomous navigation, the error amounts of and are superimposed on the heading installation error and pitch installation error respectively, and the NHC installation lever arm is set to zero. INS keeps the vehicle idle during the initial alignment period, and selects the sliding window to calculate the HCC and IMCC detection thresholds. The summary of vehicle motion state criterion thresholds is shown in TABLE 1.

The experimental results of the INS/TZV/NHC error parameter estimation prototype are shown in FIG.6. The ccelerometer zero bias converges faster, and the final estimation results of ∇_x^b, ∇_y^b, and ∇_z^b are $13.2\mu g$, $5.6\mu g$ and $-24.2\mu g$ respectively, the horizontal gyro drift ε_x^b and ε_y^bconvergence rate is slower, and the final estimation results of and are $0.0024°/h$, respectively and $-0.0023°/h$. It can be seen that the gyro drift and accelerometer bias estimation results of INS/TZV/NHC autonomous navigation system and INS/OD autonomous navigation system are relatively close. After vehicle acceleration and deceleration maneuvers, the heading installation error $\delta\alpha_\psi$ and pitch installation error $\delta\alpha_\theta$ converge rapidly, and the final estimation results are $10.2'$ and $-11.31'$, which are close to the initial superposition error; the final estimation results of the NHC installation lever arm δL_{Hx}^b, δL_{Hy}^b and δL_{Hz}^b are -0.173m, 1.296m, and 1.330m, respectively.

The experimental results of the INS/TZV/NHC autonomous navigation results are shown in FIG.7. It can be seen that the zero velocity criterion combined with HCC and IMCC can well judge the zero-velocity state of the vehicle, and the false detection rate is 0. Since the zero velocity criterion and the set threshold are relatively strict, the system will still determine that the vehicle is in a non-zero velocity

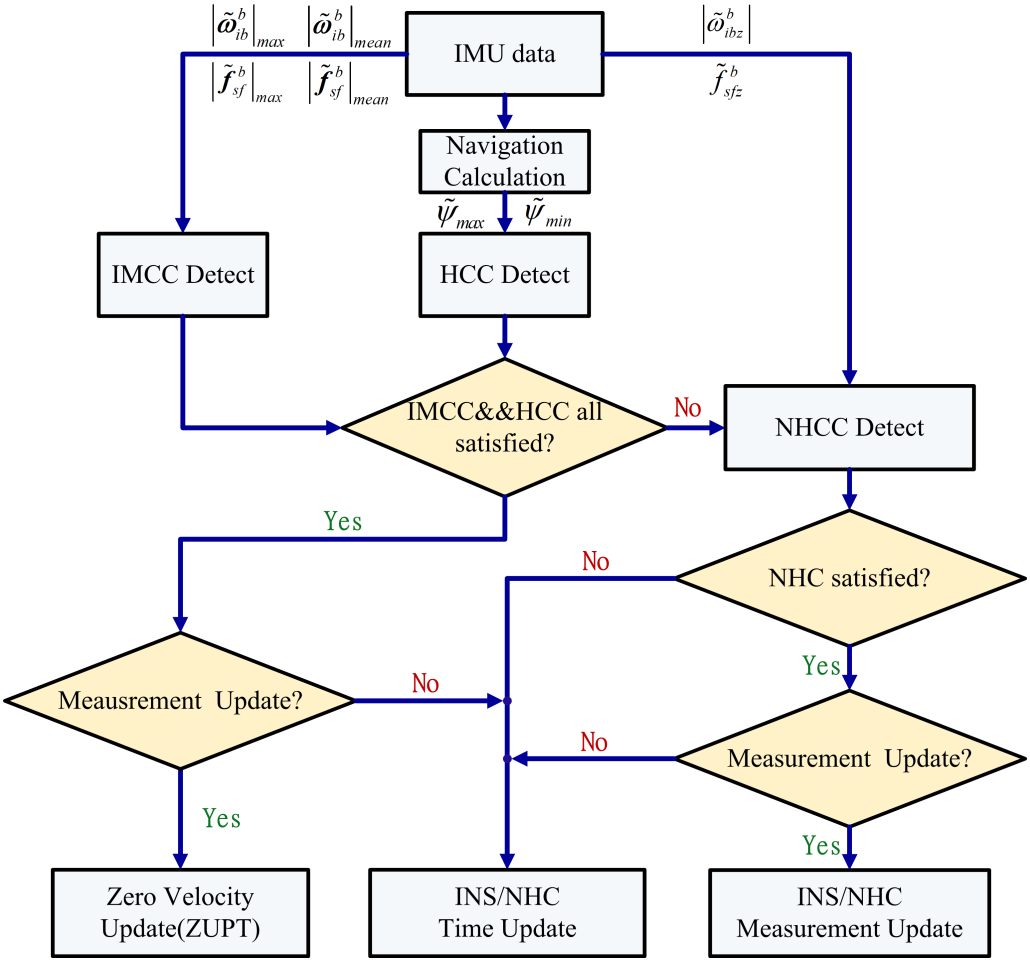

FIGURE 2. Design flow chart of INS/TZV/NHC filter algorithm based on vehicle motion state detection.

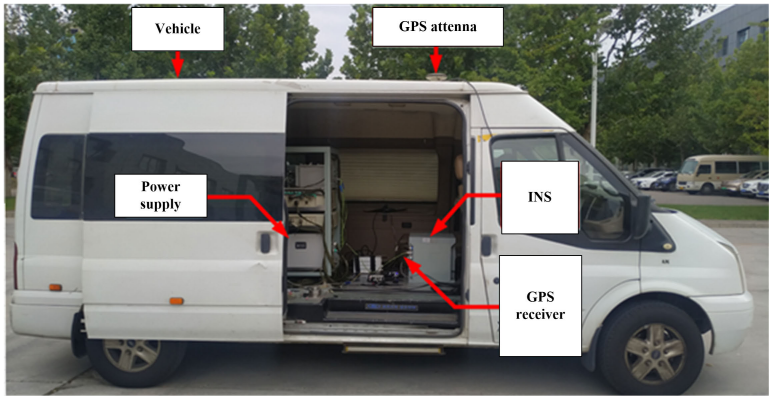

FIGURE 3. Experimental Platform.

state for some situations where the vehicle is stationary but shakes a lot. Since the system always satisfies condition C31, the measured result of the z-axis accelerometer is no longer given. It can be seen that most of the NHC information is valid for part of the time, which is beneficial to suppress the long-duration dynamic error of the INS.

Comparing the INS/TZV/NHC autonomous navigation method with the traditional INS/NHC autonomous navigation method, the eastward position error, northward position error, horizontal position error, and elevation positioning error are shown in FIG.7(a) and FIG.7(b) respectively, FIG.7(c) and FIG.7(d). It can be seen intuitively that

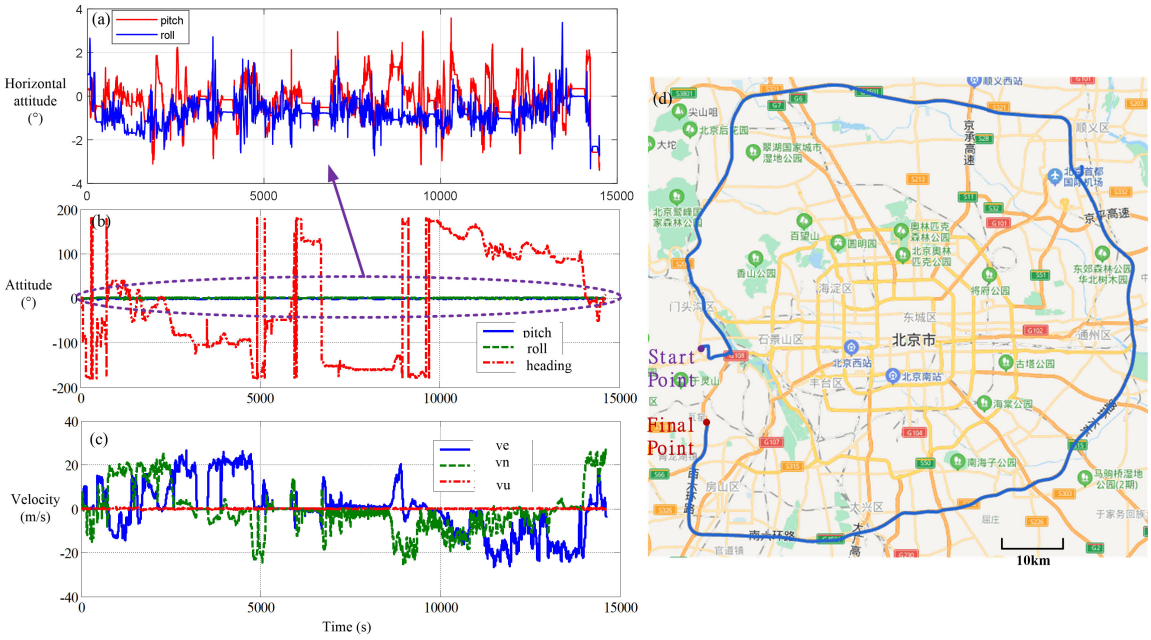

FIGURE 4. INS attitude, velocity and vehicle trajectory (path 1).

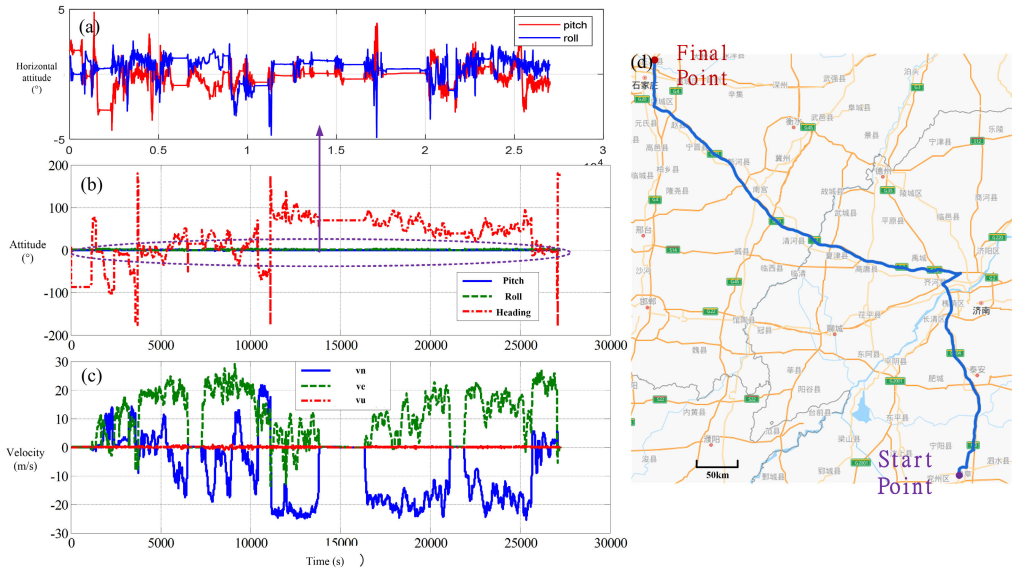

FIGURE 5. INS attitude, velocity and vehicle trajectory (path 2).

compared with the traditional INS/NHC autonomous navigation method, the proposed INS/TZV/NHC autonomous navigation method has advantages in both horizontal positioning accuracy and elevation positioning accuracy. However, during the period about 3000s to 5000s, the two methods both show a more obvious error growth trend because the vehicle approximately keeps driving along the west straight line during this period, and there is no parking point, resulting in the cumulative position error along the vehicle's driving direction because the IMU biases are not converge during this period. The superior performance of the proposed method during the period about 3000s to 5000s is because before 3000s there exists two stopping points, which has a good effect on error estimation when utilizing the proposed method. The error obtained by joint INS/NHC autonomous navigation is quickly corrected. Based on the above analysis, it can be seen that without sensor assistance, it is beneficial to make full use of TZV information to improve the positioning accuracy of the system. In path 1, the RMSE of the east position error, north position error and horizontal position

TABLE 1. Summary of motion state criterion thresholds for vehicle-mounted experimental platform.

Motion recognition pattern	Detected parameters	Thresholds
HCC	$\Delta\psi_{Th}\ ^\circ/h$	0.1mil
IMCC	$\omega_{Th,max}\ ^\circ/h$	$0.0038rad/s$
IMCC	$\omega_{Th,mean}\ ^\circ/h$	$0.0014rad/s$
IMCC	$f_{Th,max}\ ^\circ/h$	$9.969m/s^2$
IMCC	$f_{Th,mean}$	$9.806m/s^2$
NHCC	$\omega^b_{Thz,max}$	$30^\circ/s$
NHCC	$f^b_{Thz,max}$	$11.8m/s^2$
NHCC	$f^b_{Thz,min}$	$7.8m/s^2$

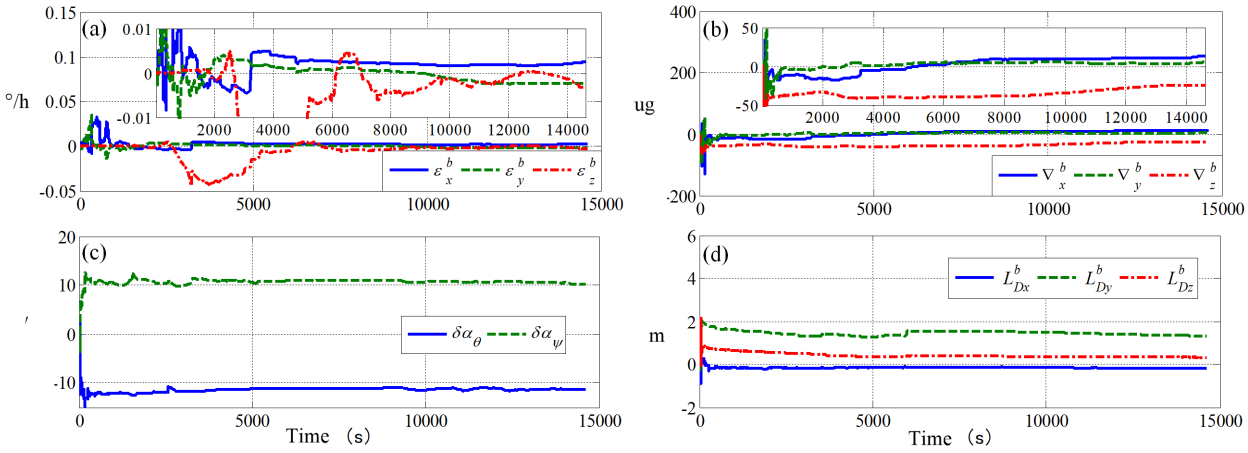

FIGURE 6. Experimental results of INS/TZV/NHC error parameter estimation prototype (path 1).

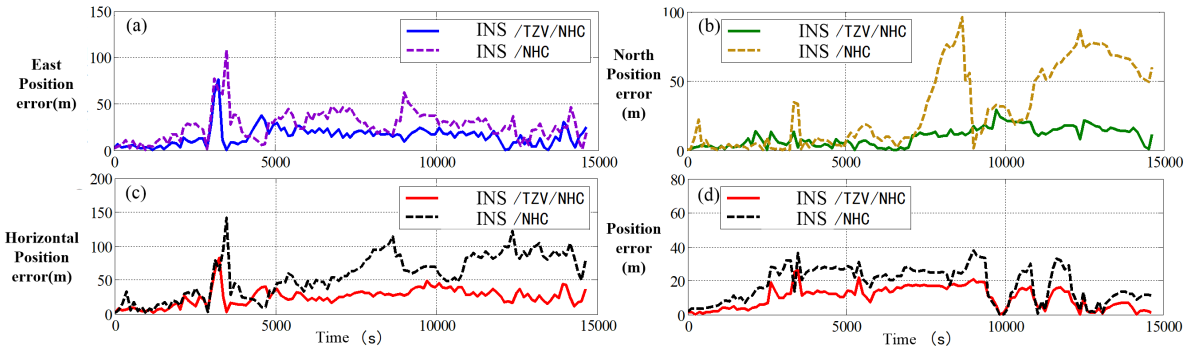

FIGURE 7. Experimental results of INS/TZV/NHC autonomous navigation results (path 1).

error utilizing the proposed method are 19.85m, 10.14m and 22.29m respectively, the RMSE of the east position error, north position error and horizontal position error utilizing the traditional INS/NHC method are 34.14m, 48.51m and 59.31m respectively.

Based on the results of experiment 1, the position error utilizing the proposed method do not increase with time when the vehicle is static, which can verify the effectiveness of the vehicle motion state judgement criterion. When the vehicle is maneuvering, the position error utilizing the proposed method is still smaller than the traditional method. This is because the criterion is more accurate, and the working mode of the INS is switched accurately, so as to obtain higher-precision positioning information. Hence, the

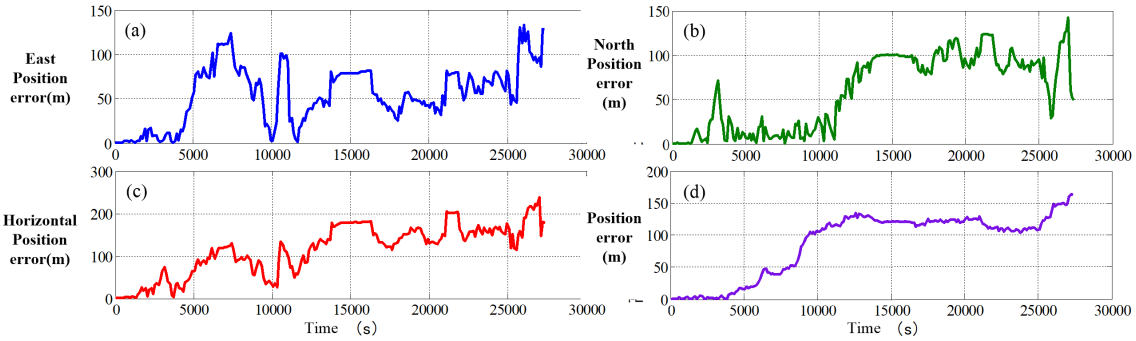

FIGURE 8. Experimental results of INS/TZV/NHC autonomous navigation results (path 2).

proposed method can achieve the accuracy level of dead reckoning without using auxiliary sensors, and solves the problem of judging the vehicle's motion state.

C. EXPERIMENT ANALYSIS OF PATH 2

The experimental results of the INS/TZV/NHC autonomous navigation prototype are shown in FIG.8. Among them, the NHC information remains valid throughout the whole process; there are many TZV information points, but the time interval of TZV information remains above 50 minutes after 3600s. At this time, the traditional ZUPT method is no longer applicable. It can be seen from the positioning error curve that in the three periods of 6550s-7300s, 13840s-16350s and 21110s-21890s, the role of TZV information is mainly to suppress The reason for the divergence of the INS positioning error is that after a long period of maneuvering, the observability has improved, and the error correction effect of the TZV information is no longer significant. Therefore, in this type of vehicle navigation scene, the INS/TZV/NHC autonomous navigation method The achieved positioning accuracy is still limited. According to the positioning error statistics, the INS/TZV/NHC autonomous navigation horizontal positioning accuracy is 80.63m (CEP), and the elevation positioning accuracy is 67.78m (PE).

V. CONCLUSION

The autonomous navigation algorithm in satellite-denied areas is an important problem in the field of land navigation. Aiming at the situation that the auxiliary equipment cannot be used, the velocity measurement model with non-integrity constraints is first introduced; on this basis, an INS/TZV/NHC filter algorithm based on vehicle motion state detection is proposed, through two zero velocity criteria and one kind of NHC information criterion, independently complete the switching of TZV and NHC measurement information, and maximize the use of known measurement information. Experimental results indicate that the proposed method can improve positioning accuracy compared with the traditional INS/NHC method, and it is more robust than INS/OD combined navigation.

However, In the case where the OD is working well, the method proposed in this paper is still difficult to exceed the INS/OD integrated navigation accuracy. We found that the deformation of the vehicle shock absorber spring will cause the installation error angle to change, which will cause the accuracy to deteriorate. Therefore, we will study the INS/NHC/TZV algorithm considering deformation in the future to further improve the accuracy.

REFERENCES

[1] Z. Wen, G. Yang, Q. Cai, and T. Chen, "An encoder-based relative attitude observation method for self-calibration in dual-axis RINS," *IEEE Trans. Ind. Electron.*, vol. 70, no. 11, pp. 11784–11794, Nov. 2023.

[2] Z. Wen, G. Yang, and Q. Cai, "An improved SINS/NHC integrated navigation algorithm based on Ackermann turning geometry," *Measurement*, vol. 192, Mar. 2022, Art. no. 110859.

[3] C. Shen, Y. Zhang, X. Guo, X. Chen, H. Cao, J. Tang, J. Li, and J. Liu, "Seamless GPS/inertial navigation system based on self-learning square-root cubature Kalman filter," *IEEE Trans. Ind. Electron.*, vol. 68, no. 1, pp. 499–508, Jan. 2021.

[4] M. Yan, Z. Wang, and J. Zhang, "Online calibration of installation errors of SINS/OD integrated navigation system based on improved NHC," *IEEE Sensors J.*, vol. 22, no. 13, pp. 12602–12612, Jul. 2022.

[5] S. Y. Cho, M. S. Chae, and K. H. Shin, "Reliability analysis of the integrated navigation system based on real trajectory and calculation of safety margin between trains," *IEEE Access*, vol. 9, pp. 32986–32996, 2021.

[6] Q. Zhang, Y. Hu, and X. Niu, "Required lever arm accuracy of non-holonomic constraint for land vehicle navigation," *IEEE Trans. Veh. Technol.*, vol. 69, no. 8, pp. 8305–8316, Aug. 2020.

[7] A. Abosekeen, A. Noureldin, and M. J. Korenberg, "Improving the RISS/GNSS land-vehicles integrated navigation system using magnetic azimuth updates," *IEEE Trans. Intell. Transp. Syst.*, vol. 21, no. 3, pp. 1250–1263, Mar. 2020.

[8] M. S. Grewal, V. D. Henderson, and R. S. Miyasako, "Application of Kalman filtering to the calibration and alignment of inertial navigation systems," in *Proc. 29th IEEE Conf. Decis. Control*, Mar. 1990, pp. 3325–3334.

[9] J. Ali and M. Ushaq, "A consistent and robust Kalman filter design for in-motion alignment of inertial navigation system," *Measurement*, vol. 42, no. 4, pp. 577–582, May 2009.

[10] J. R. Huddle, "Historical perspective on estimation techniques for position and gravity survey with inertial systems," *J. Guid., Control, Dyn.*, vol. 9, no. 3, pp. 257–267, May 1986.

[11] G. Dissanayake, S. Sukkarieh, E. Nebot, and H. Durrant-Whyte, "The aiding of a low-cost strapdown inertial measurement unit using vehicle model constraints for land vehicle applications," *IEEE Trans. Robot. Autom.*, vol. 17, no. 5, pp. 731–747, Jan. 2001.

[12] Q. Fu, Y. Liu, Z. Liu, S. Li, and B. Guan, "High-accuracy SINS/LDV integration for long-distance land navigation," *IEEE/ASME Trans. Mechatronics*, vol. 23, no. 6, pp. 2952–2962, Dec. 2018.

[13] Q. Fu, F. Wu, S. Li, and Y. Liu, "In-motion alignment for a velocity-aided SINS with latitude uncertainty," *IEEE/ASME Trans. Mechatronics*, vol. 25, no. 6, pp. 2893–2903, Dec. 2020.
[14] Q. Fu, S. Li, Y. Liu, and F. Wu, "Information-reusing alignment technology for rotating inertial navigation system," *Aerosp. Sci. Technol.*, vol. 99, Apr. 2020, Art. no. 105747.
[15] D. Bernstein and A. Kornhauser, "An introduction to map matching for personal navigation assistants," New Jersey Inst. Technol., Newark, NJ, USA, Tech. Rep., Jan. 1996.
[16] C. E. White, D. Bernstein, and A. L. Kornhauser, "Some map matching algorithms for personal navigation assistants," *Transp. Res. C, Emerg. Technol.*, vol. 8, nos. 1–6, pp. 91–108, Feb. 2000.
[17] B. P. Phuyal, "Method and use of aggregated dead reckoning sensor and GPS data for map matching," in *Proc. 15th Int. Tech. Meeting Satell. Division Inst. Navigat.*, 2002, pp. 430–437.
[18] G. Taylor, G. Blewitt, D. Steup, S. Corbett, and A. Car, "Road reduction filtering for GPS-GIS navigation," *Trans. GIS*, vol. 5, no. 3, pp. 193–207, Jun. 2001.
[19] W. Y. Ochieng, M. Quddus, and R. B. Noland, "Map-matching in complex urban road networks," *Brazilian J. Cartography*, vol. 55, no. 2, pp. 1–18, 2003.
[20] S. Syed and M. E. Cannon, "Fuzzy logic based-map matching algorithm for vehicle navigation system in urban canyons," in *Proc. Nat. Tech. Meeting Inst. Navigat.*, 2004, pp. 982–993.
[21] D. Won, J. Ahn, S. Sung, M. Heo, S.-H. Im, and Y. J. Lee, "Performance improvement of inertial navigation system by using magnetometer with vehicle dynamic constraints," *J. Sensors*, vol. 2015, pp. 1–11, Jan. 2015, doi: 10.1155/2015/435062.
[22] D. Wang, Y. Dong, Z. Li, Q. Li, and J. Wu, "Constrained MEMS-based GNSS/INS tightly coupled system with robust Kalman filter for accurate land vehicular navigation," *IEEE Trans. Instrum. Meas.*, vol. 69, no. 7, pp. 5138–5148, Jul. 2020, doi: 10.1109/TIM.2019.2955798.
[23] R. Sun, Y. Yang, K. W. Chiang, T. T. Duong, K. Y. Lin, and G. J. Tsai, "Robust IGPS/VO integration for vehicle navigation in GNSS degraded urban areas," *IEEE Sensors J.*, vol. 20, no. 17, p. 10110–10122, Sep. 2020, doi: 10.1109/JSEN.2020.2989332.
[24] L. Zhao and H. Quan, "Using regularized softmax regression in the GNSS/INS integrated navigation system with nonholonomic constraints," *IOP Conf. Ser., Mater. Sci. Eng.*, vol. 538, no. 1, May 2019, Art. no. 012058, doi: 10.1088/1757-899X/538/1/012058.
[25] Z. Wen, G. Yang, Q. Cai, and Y. Sun, "Modeling and calibration of the gyro– accelerometer asynchronous time in dual-axis RINS," *IEEE Trans. Instrum. Meas.*, vol. 70, pp. 1–17, 2021.
[26] W. Sun and Y. Yang, "BDS PPP/INS tight coupling method based on non-holonomic constraint and zero velocity update," *IEEE Access*, vol. 8, pp. 128866–128876, 2020, doi: 10.1109/ACCESS.2020.3008849.
[27] Z. Wen, G. Yang, Q. Cai, and T. Chen, "A novel Bluetooth-odometer-aided smartphone-based vehicular navigation in satellite-denied environments," *IEEE Trans. Ind. Electron.*, vol. 70, no. 3, pp. 3136–3146, Mar. 2023, doi: 10.1109/TIE.2022.3169714.
[28] Y. Zhou, Q. Chen, and X. Niu, "Kinematic measurement of the railway track centerline position by GNSS/INS/odometer integration," *IEEE Access*, vol. 7, pp. 157241–157253, 2019, doi: 10.1109/ACCESS.2019.2946981.

PEI YU received the Ph.D. degree from the China Academy of Launch Vehicle Technology, in 2020. She is currently a Lecturer with the China Fire and Rescue Institute. Her current research interests include inertial navigation and artificial intelligence application.

WEI WEI received the B.S. degree in information and computing science from the China University of Mining and Technology, Beijing, in 2010, and the M.S. degree in software engineering and the Ph.D. degree in control science and engineering from Beijing Technology and Business University, in 2013 and 2019, respectively. She is currently a Lecturer with the Information Engineering College, Beijing Institute of Petrochemical Technology. Her research interests include emotion analysis and human–machine collaboration.

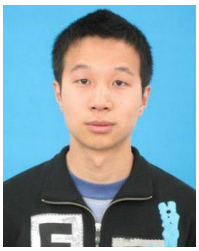

JING LI received the Ph.D. degree in optical engineering from Beihang University, Beijing, China, in 2017. He is currently a Lecturer with the Information Engineering College, Beijing Institute of Petrochemical Technology. His current research interests include machine learning and underwater signal processing.

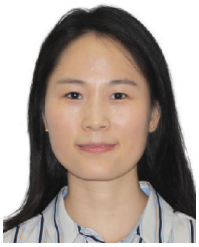

FANG WANG received the B.S. and M.S. degrees in computer science from Beijing Technology and Business University, in 2008 and 2011, respectively, and the Ph.D. degree in computer science from Beihang University, in 2017. She is currently with the Beijing Institute of Petrochemical Technology. Her research interests include data mining, knowledge engineering, and natural language processing.

LILI ZHANG received the B.S. degree in automation from the Tianjin University of Science and Technology, in 2012, and the M.S. and Ph.D. degrees in control science and engineering from the North China University of Technology University, in 2015 and 2020, respectively. He is currently a Research Assistant with the College of Information Engineering, Beijing Institute of Petrochemical Technology. His research interests include intelligent traffic signal control and traffic simulation, the Internet of Vehicles, and artificial intelligence.

ZENGQIANG CHEN received the B.S. degree in information and computing science, the M.S. degree in applied mathematics, and the Ph.D. degree in control theory and control engineering from the Beijing University of Chemical Technology, in 2006, 2009, and 2013, respectively.